JACS
JOURNAL OF THE AMERICAN CHEMICAL SOCIETY

Article

pubs.acs.org/JACS

An Orange Fluorescent Protein with a Large Stokes Shift for Single-Excitation Multicolor FCCS and FRET Imaging

Daria M. Shcherbakova,[†,§] Mark A. Hink,[‡,§] Linda Joosen,[‡] Theodorus W. J. Gadella,[‡] and Vladislav V. Verkhusha*[,†]

[†]Department of Anatomy and Structural Biology and Gruss-Lipper Biophotonics Center, Albert Einstein College of Medicine, 1300 Morris Park Avenue, Bronx, New York 10461, United States

[‡]Swammerdam Institute for Life Sciences, Section of Molecular Cytology, van Leeuwenhoek Centre for Advanced Microscopy, University of Amsterdam, Science Park 904, NL-1098 XH, Amsterdam, The Netherlands

Supporting Information

ABSTRACT: Multicolor imaging based on genetically encoded fluorescent proteins (FPs) is a powerful approach to study several dynamic processes in a live cell. We report a monomeric orange FP with a large Stokes shift (LSS), called LSSmOrange (excitation/emission at 437/572 nm), which fills up an existing spectral gap between the green-yellow and red LSSFPs. Brightness of LSSmOrange is five-fold larger than that of the brightest red LSSFP and similar to the green-yellow LSSFPs. LSSmOrange allows numerous multicolor applications using a single-excitation wavelength that was not possible before. Using LSSmOrange we developed four-color single-laser fluorescence cross-correlation spectroscopy, solely based on FPs. The quadruple cross-correlation combined with photon counting histogram techniques allowed quantitative single-molecule analysis of particles labeled with four FPs. LSSmOrange was further applied to simultaneously image two Förster resonance energy transfer pairs, one of which is the commonly used CFP-YFP pair, with a single-excitation laser line. The combination of LSSmOrange-mKate2 and CFP-YFP biosensors enabled imaging of apoptotic activity and calcium fluctuations in real time. The LSSmOrange mutagenesis, low-temperature, and isotope effect studies revealed a proton relay for the excited-state proton transfer responsible for the LSS phenotype.

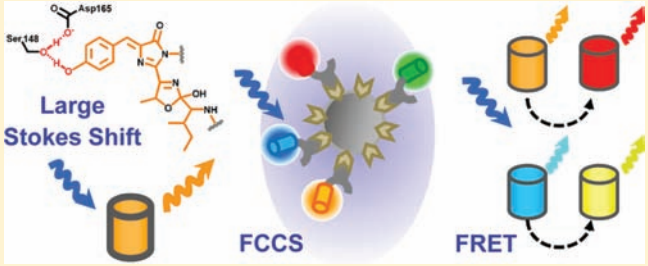

1. INTRODUCTION

Multicolor imaging using fluorescent proteins (FPs) is a powerful approach to study molecular processes in live cells. Despite the availability of different FP variants,[1,2] full exploration of multiplexed colocalization and interaction analyses still requires development of fluorescent probes with novel spectral properties. Of special interest are approaches that exploit a single-excitation wavelength for a set of fluorescent probes with resolvable emission spectra. Among these are single-laser (SL) fluorescence cross-correlation spectroscopy (FCCS)[3] and Förster resonance energy transfer (FRET) using one excitation wavelength for simultaneous imaging of several biosensors in a cell.[4,5]

FCCS technique using FPs can be potentially expanded to study interaction of more than two proteins. Comparing to FRET, FCCS is not highly affected by the distance and relative orientation between the interacting probes.[6,7] Moreover, FCCS can be applied to study interaction between several proteins, whereas FRET is generally limited to two, maximally three interacting species.[8,9] In conventional dual-color FCCS assays employing two different FPs, alignment of two lasers to the same confocal spot is often challenging. This problem can be overcome in two ways. The first approach utilizes a SL two-photon excitation (2PE) because of the broad excitation spectra of fluorescent probes in 2PE mode.[10] The second approach uses FPs, which can all be excited with a SL and yet display well-separable emission spectra.[6,11] Although 2PE-SL-FCCS has been applied,[10] it required an expensive two-photon laser and led to complex photobleaching artifacts.[12] Until now, multicolor SL-FCCS utilizing FPs has been limited to two FPs.[6,11] SL-FCCS with more than two colors has been applied to synthetic dyes in solution only.[13−15] Therefore, design of FPs with a large Stokes shift with excitation maxima close to those of conventional FPs but with red-shifted emission spectra is required to perform triple or quadruple SL-FCCS and apply this technique to study higher order molecular complexes.

FRET-based biosensors are widely used to study dynamics of second messengers, protein−protein interactions, enzyme activities, and ion concentration changes.[16,17] With many FRET biosensors available, their combined use is desirable to achieve temporal and spatial resolution of several events in the same cell.[4,5] The most widely used are FP-based single-chain ratiometric biosensors. Ratiometric imaging is preferable since its readout is insensitive to dye concentration and is easy to quantify. However, spectral properties of the majority of existing FRET

Received: February 26, 2012
Published: April 9, 2012

dx.doi.org/10.1021/ja3018972 | J. Am. Chem. Soc. 2012, 134, 7913−7923

pairs limit simultaneous detection of multiple FRET sensors because of the spectral overlaps. In order to circumvent this problem, researchers use intensiometric imaging, apply fluorescence lifetime-based FRET, utilize FRET acceptors with poor quantum yield (quenchers), share one acceptor between two FRET pairs, or use organic dyes (reviewed in refs 4 and 5).

Recently, dual FRET imaging of two ratiometric biosensors has been reported.[18−20] However, a FRET pair that is spectrally compatible with the common CFP-YFP pair and could be efficiently excited with the same laser is still highly required. Currently available FPs with a large Stokes shift (LSS) include green T-Sapphire,[21] yellow mAmetrine,[18] and red LSSmKate1,[22] LSSmKate2,[22] and mKeima[11] proteins. Orange LSSFP is missing in this palette. Moreover, the existing red LSSFPs suffer from low brightness.

Development of an orange FP with a large Stokes shift (LSSFP) to fill up the gap in the LSSFP colors and to serve as an efficient FRET donor for far-red FPs could provide a solution to all these problems. Here, we designed the first orange LSSFP and applied it to the four-color SL-FCCS and simultaneous dual FRET SL imaging.

2. EXPERIMENTAL PROCEDURES

2.1. Mutagenesis and Screening of Libraries. The mOrange gene[23] was amplified by polymerase chain reaction (PCR) as the *Bgl*II-*Eco*RI fragments using PCR and inserted into a pBAD/His-B vector (Invitrogen). Site-specific mutagenesis was performed using a QuickChange mutagensis kit (Stratagene). For simultaneous mutagenesis at several positions, an overlap−extension approach was applied.[24] Random mutagenesis was performed with a GeneMorph II random mutagenesis kit (Stratagene) using conditions that resulted in the mutation frequency of up to 16 mutations per 1000 base pairs. After the mutagenesis, a mixture of mutated genes was electroporated into LMG194 bacterial host cells (Invitrogen).

Libraries of 10^6−10^7 independent clones of mOrange mutants were screened using a MoFlo (Dako) fluorescence-activated cell sorter (FACS) followed by colony visualization using Leica MZ16F fluorescence stereomicroscope, as previously described.[22] The stereomicroscope was equipped with 436/20 and 540/20 nm excitation and 575/30 nm emission filters (Chroma). In sorting as a negative selection, we used 530 nm mixed gas excitation laser line with 570 nm long-pass emission filter, 488 nm Ar excitation laser line with 510/21 emission filter, and 407−413 nm Kr excitation line with 510/21 emission filter. As a positive selection, we used 407−413 nm Kr excitation line with 570 nm long-pass emission filter. The 20−30 brightest clones were chosen and sequenced. Clones containing external mutations possibly leading to dimerization[25] were excluded. Mixtures of selected variants were used as templates for the next round of random mutagenesis.

2.2. Protein Characterization. T-Sapphire, mAmetrine, mKeima, LSSmKate1, LSSmKate2, and LSSmOrange mutant proteins with polyhistidine tags were expressed in LMG194 bacteria grown in a RM medium supplemented with 0.002% arabinose for 24−48 h at 37 °C and then purified using a Ni-NTA agarose (Qiagen). Excitation and emission spectra of recombinant proteins were measured with a FluoroMax-3 spectrofluorometer (Jobin Yvon). For absorbance measurements, a Hitachi U-3010 spectrophotometer was used.

The concentrations of proteins were determined using a BCA protein assay kit (Pierce). To determine extinction coefficients, we relied on measuring the mature chromophore concentration, as described previously.[22] In brief, the purified FPs were alkali denatured. It is known that the extinction coefficient of a GFP-like chromophore is 44 000 M^{-1} cm^{-1} at 446 nm in 1 M NaOH.[26] Based on the absorbance of the native and denatured proteins, molar extinction coefficients for the native states were calculated. To determine quantum yields, the fluorescence intensities of protein solutions were compared to the fluorescence intensities of equally absorbing amounts of LSSmKate2 (quantum yield is 0.17). Equilibrium pH titrations were performed using a series of buffers (100 mM NaOAc and 300 mM NaCl for pH 2.5−5.0 and 100 mM NaH_2PO_4 and 300 mM NaCl for pH 4.5−9.0).

To study protein maturation, LMG194 bacterial cells transformed with the LSSFP genes were grown in RM medium supplemented with ampicillin at 37 °C overnight. The next morning, bacterial cells were diluted to optical density 1.0 at 600 nm, and 0.2% arabinose was added. Upon induction of protein production, bacterial cultures were grown at 37 °C in 50 mL tubes filled to the brim and tightly sealed to restrict oxygen supply. After 1 h, the cultures were centrifuged in the same tightly closed tubes. After opening the tubes, the proteins were purified using the Ni-NTA resin within 30 min, with all procedures and buffers at or below 4 °C. Protein maturation was conducted in PBS at 37 °C. Fluorescence emission signal of the maturing proteins was monitored using the FluoroMax-3 spectrofluorometer.

Photobleaching kinetics was measured using purified proteins in PBS at 1 mg/mL in aqueous drops in oil using an Olympus IX81 inverted microscope equipped with a 200 W metal halide arc lamp (Prior), a 100× 1.4 NA oil immersion objective lens (UPlanSApo, Olympus). For LSSmOrange, LSSmKate1, and LSSmKate2, 436/20 nm excitation and 575/30 nm emission filters were used. For T-Sapphire and mAmetrine 390/40 nm excitation and 535/40 emission filters were used. All filters were from Chroma. The microscope was operated with SlideBook 4.2 software (Intelligent Imaging Innovations). The data were normalized to a spectral output of the lamp, transmission profiles of the excitation filter and the dichroic mirror, and absorbance spectra of the LSSFPs. LSSmKate1 was used as a reference.

For proton-transfer studies, exchangeable protons in LSSmOrange sample were replaced with deuterium by repeated dilution of the protein with PBS/glycerol (1:1 by v/v) buffer in D_2O followed by concentration by ultracentrifugation. For isotope effect studies, samples were analyzed in PBS/glycerol (1:1 by v/v).

2.3. Flow Cytometry of Bacterial Cells. Bacteria transformed with LSSmOrange, LSSmKate1, T-Sapphire, or TagBFP2 were analyzed by a FACSAria cell sorter equipped with a solid-state 407 nm laser and 3 PMT detectors. Two detectors and two emission band-pass filters (546/10 and 610/20) were used to detect transformed bacteria. The 15 000 events for each type of transformed bacteria were analyzed. All four types of bacteria were run under the same conditions in one experiment. For data analysis, FlowJo software (Tree Star) was used. Obtained dot plots for each type of transformed bacteria were superimposed.

2.4. Mammalian Plasmid Construction. To construct pLSSmOrange-N1 and mOrange-N1 plasmids, the corresponding gene of fluorescent protein was PCR amplified as *Age*I-*Not*I fragments and swapped with EGFP gene in a pEGFP-N1 vector (Clontech). To construct pLSSmOrange-C1 plasmid, LSSmOrange was PCR amplified as a *Nhe*I-*Bgl*II fragment and swapped with an EGFP gene in a pEGFP-C1 vector (Clontech).

To construct pLSSmOrange-β-actin and pLSSmOrange-α-tubulin, the LSSmOrange gene was PCR amplified and swapped with a mTagBFP gene in pmTagBFP-β-actin and pmTagBFP-α-tubulin plasmids.[27] To construct pKeratin-LSSmOrange, pVimentin-LSSmOrange, pα-Actinin-LSSmOrange, pH2B-LSSmOrange, pH2B-mOrange, pMito-LSSmOrange, and pMito-mOrange, the LSSmOrange or mOrange gene was cut from the pLSSmOrange-N1 or pmOrange-N1 plasmids and swapped with the mTagBFP gene in the pKeratin-TagBFP, pVimentin-TagBFP, pα-Actinin-TagBFP, pH2B-TagBFP, and pMito-TagBFP plasmids. The mTagBFP containing plasmids were provided by M.W. Davidson, Florida State University.

2.5. Mammalian Cell Culture, Transfection, and Imaging. HeLa cells were cultured in DMEM medium supplemented with 10% FBS and 0.5% penicillin-streptomycin (all from Invitrogen). Transfections were performed with the plasmids indicated above using an effectene reagent (Qiagen), as described in the manufacturer's protocol. In brief, HeLa cells were seeded on 25 mm glass coverslips in a 6-well plate resulting in 40% confluency the following day. The preincubated mixture of 0.4 μg DNA with the effectene and

supplementary reagents were added to the cells. After 24 h, the growth media with the effectene−DNA complexes was replaced by a fresh one.

Imaging of the LSSmOrange and mOrange fusions in live HeLa cells was performed 48−72 h after the transfection. The cells were imaged using an Olympus IX81 inverted microscope equipped with a 200 W metal-halide lamp and a 100× 1.4 NA oil immersion objective lens (UPlanSApo, Olympus) and either with one filter set (436/20 nm exciter, 575/30 emitter) for LSSmOrange fusions alone or with a combination of two filter sets (390/40 nm exciter, 605/40 nm emitter; and 540/20 nm exciter, 575/30 nm emitter) for two-color imaging of cells cotransfected with LSSmOrange and mOrange fusions. All filter sets were from Chroma. A SlideBook v.4.1 software (Intelligent Imaging Innovations) was used to operate the Olympus IX81 microscope.

2.6. Characterization of FRET Caspase-3 Biosensor. The LSSmOrange-mKate2 fusion constructs containing an N-terminal strep tag (amino acids −WSHPQFEK−) and a C-terminal polyhistidine tag were cloned as *Nco*I-*Xba*I fragments into a pBAD/Myc-His B vector (Invitrogen). The fusions contained a 20 amino acid linkers with the caspase-3 recognition site (−EFGGSGS-DEVDKLGGSGSGT−). In vitro characterization was performed as described previously.[27] In brief, the fusion was expressed in LMG194 bacterial cells overnight at 37 °C and isolated with an Ni-NTA agarose (Qiagen) followed by the additional purification with a strep-tactin sepharose (IBA). The purified construct at concentrations 100 μg/mL was digested with 30 μg/mL of trypsin for 2 h at 37 °C. Emission spectra during this time were measured with a FluoroMax-3 spectrofluorometer (Jobin Yvon).

LSSmOrange-mKate2 caspase-3 biosensor for production in mammalian cells was constructed as follows: The LSSmOrange gene was PCR amplified from a pBAD/Myc-HisB vector containing the LSSmOrange-mKate2 fusion. A 5′-primer contained *Bgl*II site at the end followed by the Kozak sequence and N-terminal GFP-end encoding sequence. A 3′-primer contained sequence encoding the DEVDKLGGSGSGT amino acids for a cleavable (cleavage site is underlined) and the SASGKLGGSGSGT amino acids for a non-cleavable (substitution sequence is underlined) fusions followed by an *Age*I site. PCR product was digested with *Bgl*II and *Age*I and inserted into the digested with same restriction enzymes pmKate2-N1 vector.

2.7. Dual FRET Imaging and Analysis. HeLa cells were cotransfected with plasmids encoding yellow cameleon calcium biosensor YC3.60[28] and LSSmOrange-mKate2 caspase-3 biosensor, cleavable or noncleavable. Cells were grown in DMEM supplemented with glutamax (Gibco) containing 10% FBS and 0.5% penicillin-streptomycin (Invitrogen). Approximately 5.0×10^5 HeLa cells were seeded at 25 mm round no. 1 coverslips (Menzel) placed in 6-well plates (Greiner). The following day the cells were transfected using lipofectamine in OptiMEM medium (Invitrogen). 48−72 h after transfection, the coverslips were sealed in an attofluor cell chamber (Invitrogen) submerged in imaging medium (20 mM HEPES (pH = 7.4), 137 mM NaCl, 5.4 mM KCl, 1.8 mM $CaCl_2$, 0.8 mM $MgCl_2$, and 20 mM glucose). Cells were treated with 1 μM histamine (LC Laboratories) after 5 min and either 20 ng/mL TNF-α or 2 μM staurosporine after 30 min from the start of the experiment. Cell samples were imaged using an A1-confocal microscope equipped with a spectral detector (Nikon). Excitation light of a 440 nm laser diode was focused via a 20/80 dichroic mirror by a 60× oil immersion objective lens (PlanApoVC 1.40 NA) into the sample. Fluorescence was detected with a spectral detector consisting of 29 PMTs, set at a gain of 160 and detecting fluorescence signal between 450 and 740 nm with a 10 nm spectral bandwidth per PMT. Multiple spots of cells were imaged sequentially using 16× averaging up to 5 h as controlled by the NIS Elements v.3.22 acquisition software (Nikon).

The Nikon nd2 spectral data sets were analyzed using the in-house written macros (available upon request) for the ImageJ v.1.45k software (http://rsbweb.nih.gov/ij/) using the LOCI tools v.4.3.1, SyncWindows v.1.5, Spectral Unmixing v.1.5, and Jama v.1.0.1 plugins. Spectral unmixing was done considering four reference spectra: YC3.6-calcium free ($R_1(\lambda)$), YC3.6 calcium bound ($R_2(\lambda)$), cleaved LSSmOrange-mKate2 caspase-3 ($R_3(\lambda)$), and intact LSSmOrange-mKate2 caspase-3 ($R_4(\lambda)$). The reference spectra were obtained by measuring single-transfected HeLa cells incubated in imaging medium with or without YC3.6 activators (10 μM ionomycin or 1 μM histamine (Sigma)) and caspase-3 activators (2 μM staurosporine or 20 ng/mL TNF-α (LC Laboratories)).

The spectrum $S(\lambda)$ of a pixel in an image contains contributions a_i of each reference spectrum:

$$S(\lambda) = \sum_{i=1}^{4} a_i R_i(\lambda) \tag{1}$$

The unmixed components, a_i, are found by matrix inversion:

$$a_i = \mathbf{A}^{-1} X_i \tag{2}$$

In which the element of the uninverted matrix $\mathbf{A}$ $a_{ik} = \sum_\lambda R_i(\lambda) R_k(\lambda)$ and $X_i = \sum_\lambda S(\lambda) R_i(\lambda)$. Fractions of Ca^{2+}-bound YC3.6 and cleaved caspase-3 biosensor are retrieved from

$$F_{\mathrm{YC3.6(Ca^{2+}\text{-}bound)}} = a_2/(a_1 + a_2) \tag{3}$$

$$F_{\mathrm{caspase\text{-}3(cleaved)}} = a_3/(a_3 + a_4) \tag{4}$$

For one pixel there was a correlation of 99.98% between original and remixed data, with an overall residual of 1.1%.

2.8. FCCS Measurements and Preparation of Samples. Measurements were performed on an inverted Fluoview-1000 laser scanning microscope (Olympus). The excitation light of a 440 nm 20 MHz pulsing laser diode (Picoquant) (controlled by a Sepia-II laser driver unit (Picoquant)) was attenuated 10-fold by a neutral density filter. The light was guided via a D440/514/594 primary dichroic mirror (Chroma) through a 60× water immersion objective lens (UPlanSApo, 1.2 NA) into the sample. Samples were stored in blackened glass-bottomed 96-well plates (Whatman). The emission light was guided via a size-adjustable pinhole, set at 120 μm, through the Olympus detection box to the fiber-coupled output channel. The optical fiber was coupled to a custom-made detection box (Picoquant) containing four PDM avalanche photodiodes (MPD). A secondary D560 dichroic mirror (Semrock) was used to split the emission and two tertiary dichroic mirrors, D510 and D595 (Semrock), allowing to further split the emission light into four different colors with each channel filtered by a specific emission filter in front of the detector: 475/45 (mTagBFP2), 525/45 (T-Sapphire), 562/40 (LSSmOrange), and 641/75 (LSSmKate1) (Semrock). The photon arrival times were recorded by a Picoharp-300 time-correlated single-photon counting system (Picoquant).

Samples were diluted and mixed in PBS and measured at room temperature (21 °C). A suspension of 10 nM protein A labeled Micromer beads of 100 nm diameter (Micromod) were mixed with 120 nM mouse immunoglobulin gamma (IgG2a κ) anti-His (MBL) in PBS containing 4 mg/mL BSA (PBS-BSA) and incubated for 15 min at room temperature. Unbound IgGs were then washed away using centrifugal filter units with a molecular weight limit of 100 kDa. After three washes with PBS-BSA, the bead−antibody complexes were resuspended in 200 μL PBS and mixed with solutions of FPs with various concentrations. For stoichiometric bead measurements, the degree of bead labeling was chosen to be maximally 20 FP molecules per bead. The degree of labeling was validated by an extension of photon counting histogram (PCH) analysis,[29] as described below. For all other experiments the average degree of labeling was chosen to be less than 1 FP per bead to minimize FRET and heterogeneity among particles. Unbound FPs were washed away using a centrifugal filter unit with a molecular weight limit of 70 kDa, after that the samples were measured immediately.

The photon arrival times were recorded during 120−240 s by the SymPhoTime v.5.13 (Picoquant) software. The size, shape, and overlap of the four observation volumes were determined on a daily basis from FCCS measurements of the calibration dyes Atto425 and Alexa488 QDot565 ITK amino PEG and QDot 655 ITK amino PEG and 0.1 μm diameter TetraSpeck beads (Invitrogen).

dx.doi.org/10.1021/ja3018972 | J. Am. Chem. Soc. 2012, 134, 7913−7923

2.9. FCCS Data Analysis. The raw intensity data was auto- and cross-correlated and analyzed using the FFS Dataprocessor v.2.3 software (SSTC). The four channel cross-correlation analysis was performed in MatLab v.R2009a (MatWorks).

Auto- and dual-channel cross-correlation curves, $G_{ij}(\tau)$, were generated from the raw intensity traces I in detection channels i and j:

$$G_{ij}(\tau) = 1 + \frac{<\delta I_i(t)\cdot I_j(t+\tau)>}{<I_i>\cdot<I_j>} \quad \text{with } i = j \text{ for autocorrelation}) \tag{5}$$

Here $<I_i>$ denotes the average intensity in channel i, and $\delta I_i(t)$ is the time-dependent deviation from the average. Autocorrelation curves of the blue, green, orange, or red detection channels were fitted between 100 μs and 100 ms according to a diffusion model as in[30]

$$G_{ij}(\tau) = 1 + \left(1 - \frac{I_{i,\text{background}}}{I_{i,\text{total}}}\right)\cdot\left(1 - \frac{I_{j,\text{background}}}{I_{j,\text{total}}}\right)\cdot \left(\frac{1}{<N>}\cdot\frac{1 - T + Te^{(-\tau/\tau_T)}}{(1-T)}\cdot\frac{1}{\left(1+\frac{\tau}{\tau_{\text{dif}}}\right)\sqrt{1+\frac{\tau}{\text{sp}^2\cdot\tau_{\text{dif}}}}}\right) \tag{6}$$

where T represents the fraction of molecules in the dark state and τ_T the relaxation rate of this dark state. The diffusion time of the fluorescent particles, τ_{dif}, depends on the shape of the observation volume, sp, that is defined as the ratio of the axial (ω_z) over the radial axis (ω_{xy}). The particle number, N, retrieved from this analysis can be corrected for background fluorescence, $I_{\text{background}}$, using the first two terms between brackets in eq 6.

The amplitude of the dual-channel cross-correlation curve, $G_{ij}(0)$, scales linearly to the number of the double-colored particles, N_{ij}:[31]

$$N_{ij} = \frac{G_{ij}(0) - 1}{(G_{ii}(0) - 1)\cdot(G_{jj}(0) - 1)} \tag{7}$$

For a system consisting of four colors in the blue (b), green (g), orange (o), and red (r), the cross-correlation analysis can be extended to three[32] or four channels:

$$G_{\text{bgor}}(\tau, \tau', \tau'') = \frac{<\delta I_b(t)>\cdot<\delta I_g(\tau)>\cdot<\delta I_o(\tau')>\cdot<\delta I_r(\tau'')>}{<I_b(t)>\cdot<I_g(t)>\cdot<I_o(t)>\cdot<I_r(t)>} \tag{8}$$

The amplitude of the quadruple-correlation function:

$$G_{\text{bgor}}(0,0,0) = \frac{<\delta N^4_{\text{bgor}}(t)>}{<N_{b,\text{tot}}>\cdot<N_{g,\text{tot}}>\cdot<N_{o,\text{tot}}>\cdot<N_{r,\text{tot}}>} \tag{9}$$

Since particles were measured at low concentrations and behave independently of each other, the probability to detect any particle species, like the quadruple labeled one, N_{bgor}, follows Poissonian statistics. Thus, the fourth central moment of the Poissonian distributed $N_{\text{bgor}}(t)$ can be rewritten to

$$G_{\text{bgor}}(0,0,0) = \frac{<N_{\text{bgor}}>}{<N_{b,\text{tot}}>\cdot<N_{g,\text{tot}}>\cdot<N_{o,\text{tot}}>\cdot<N_{r,\text{tot}}>} \tag{10}$$

The number of quadruple-labeled particles, N_{bgor}, can be derived from the quadruple-correlation and autocorrelation amplitudes as

$$N_{\text{bgor}} = \frac{G_{\text{bgor}}(0,0,0) - 1}{(G_{bb}(0) - 1)\cdot(G_{gg}(0) - 1)\cdot(G_{oo}(0) - 1)\cdot(G_{rr}(0) - 1)} \tag{11}$$

2.10. Correlation Corrections in FCCS. In general, resulting particle numbers have to be corrected for background fluorescence, the nonperfect overlap of the detection volumes and spectral cross-talk. The background correction could be ignored in these experiments since the background intensities (Table S1, Supporting Information) were more than 15× lower than the sample intensities. We measured the overlap of the detection volumes for SL-FCCS to be 95−99%, in contrast to 55−85% for 'conventional' FCCS with four different excitation lasers. The resulting particle numbers can be converted into concentration values by division through the size of the various auto- or cross-correlation observation volumes, as determined from calibration measurements (see below).

Cross-talk increases the apparent number of molecules retrieved from autocorrelation analysis and can result in false-positive cross-correlating particles. Therefore, all correlation curves need to be corrected. For appropriate correction, the molecular brightness values of all correlating dyes contributing to a detection channel should be taken into account. To estimate cross-talk intensity factors and molecular brightness, the fluorescence intensity and autocorrelation curves were determined in solutions of purified protein and single-labeled beads with an average label density below 1 (Table S1, Supporting Information).

Noncorrelating cross-talk can be considered a steady 'background' and the first two terms between brackets in eq 6 can be used to correct the data. In the autocorrelation curve, each dye contributes to the curve by a product of the molar fraction Y_{dye} and the square of its (relative) molecular brightness $\eta_{\text{dye,det}}$ in that detection channel:

$$N^{\text{det,dye}}_{\text{corrected}} = \frac{N^{\text{det}}_{\text{fit}}}{\sum_{\text{dyes}}\Phi_{\text{dye,det}}} \quad \text{with} \quad \Phi_{\text{dye,det}} = \frac{(\eta^2_{\text{dye,det}}Y_{\text{dye}})}{(\sum_{\text{dyes}}\eta_{\text{dye,det}}Y_{\text{dye}})^2} \tag{12}$$

2.11. Brightness Analysis of the Labeled Beads. The label density of the beads was validated by photon counting distribution analysis in FFS Data Processor v.2.3 software (SSTC). The analysis is based on the photon counting histogram analysis[29] extended with multiple distribution analysis, analog to the method used by Palo et al.,[33] including fitting corrections for nonideal Gaussian detection volumes, dark-state kinetics, diffusion, and background.[34,35] The data were binned in time windows of 0.01, 0.1, 1, 10, and 50 ms and analyzed using an one-component 3D diffusion model.[29] To improve fitting speed and quality, similar parameters were linked. The parameters for diffusion (τ_{dif}), dark-state kinetic time (τ_T), volume structure parameter (sp), and particle number (N) were globally linked to the same parameters of the corresponding autocorrelation curve that was fitted simultaneously using a standard diffusion model (eq 6). The analysis was calibrated for monomeric molecular brightness, using solutions of free purified proteins and beads with an average label density below 1.

3. RESULTS

3.1. Development of LSSmOrange. To develop orange FP with LSS, we applied rational design in combination with directed molecular evolution to mOrange template[23] (ex/em 548/562 nm). Point mutations mOrange/165D/167L and mOrange/165A/160E were introduced into mOrange gene to create LSS phenotype with excitation in a cyan region of the spectrum.[36] To develop a protein without the excitation peak of parental mOrange, a mixture of these mutants was subjected to several rounds of random mutagenesis using an error-prone polymerase chain reaction. Bacterial libraries of 10^7−10^8 clones of mutants were subjected to high-throughput screening using a fluorescence-activated cell sorter (FACS) followed by selection of the appropriate clones on Petri dishes using fluorescent stereomicroscope. Bright LSS orange fluorescence was used as the positive criterion for selection, while orange fluorescence with a regular Stokes shift (that is typically 15−45 nm for FPs) and fluorescence in other spectral regions were used as the negative criteria. The final variant, called LSSmOrange (ex/em 437/572 nm), had A44 V, F84L, W145M, I165D, M167L,

dx.doi.org/10.1021/ja3018972 | J. Am. Chem. Soc. 2012, 134, 7913−7923

Table 1. Properties of Purified LSSmOrange in Comparison with Other Available FPs with a Large Stokes Shift[a]

protein	excitation maximum (nm)	emission maximum (nm)	extinction coefficient (M^{-1} cm^{-1})	quantum yield	brightness relative to T-Sapphire	photostability half-time (s)	p*Ka*	maturation half-time at 37 °C (h)
T-Sapphire	399	511	44 000	0.60	1.00	9	5.7	1.3
mAmetrine	406	526	45 000	0.58	0.99	10	6.2	0.8
LSSmOrange	437	572	52 000	0.45	0.89	10	5.7	2.3
LSSmKate2	460	605	26 000	0.17	0.17	25	2.7	2.5
mKeima	440	620	13 400	0.24	0.12	9	6.0	4.4
LSSmKate1	463	624	31 200	0.08	0.09	35	2.7	1.8

[a]All spectroscopic parameters were determined in PBS at pH 7.4.

G202D substitutions relative to parental mOrange (numbering follows that for EGFP, Figure S1, Supporting Information). A single external to protein β-barrel mutation G202D possibly improved LSSmOrange folding.[37]

3.2. Properties of LSSmOrange. We characterized LSSmOrange and compared its properties with those of T-Sapphire (ex/em 399/511 nm), mAmetrine (ex/em 406/526 nm), LSSmKate1 (ex/em 463/624 nm), LSSmKate2 (ex/em 460/605 nm) and mKeima (ex/em 440/620 nm) (Table 1). Normalized spectra of the LSSFPs are shown in Figure 1A. An excitation spectrum of LSSmOrange has a single excitation peak similarly to that for mAmetrine, LSSmKate1, and LSSmKate2. In contrast, T-Sapphire and mKeima revealed additional peaks corresponding to regular Stokes shift phenotypes[36] (Figure 1A).

The molar extinction coefficient and quantum yield of LSSmOrange were 52 000 M^{-1} cm^{-1} and 0.45, respectively (Table 1). LSSmOrange had a brightness (product of the extinction coefficient and quantum yield) substantially higher than that of red LSSFPs and comparable to that of green-yellow LSSFPs (Figure 1B). Notably, LSSmOrange exhibited 5.3-fold brighter fluorescence than LSSmKate2.

LSSmOrange fluorescence had a p*Ka* value of 5.7 (Table 1; Figure S2A, Supporting Information). Chromophore maturation half-time at 37 °C was 2.3 h (Figure S2B, Supporting Information). Photostability of LSSmOrange and other LSS FPs were compared in aqueous drops of the purified proteins in oil under wide-field illumination. The raw photobleaching data were normalized to absorbance spectra of the proteins, spectra of the arc lamp, and filter transmission. Normalized LSSmOrange photostability was similar to that of T-Sapphire, mAmetrine, and mKeima (Figure S2C, Supporting Information). In seminative polyacrylamide gel, LSSmOrange had the mobility similar to that of the monomeric control (Figure S3, Supporting Information).

3.3. Multicolor Labeling of a Live Cell. To characterize LSSmOrange in mammalian cells, we expressed LSSmOrange fusion constructs in HeLa cells. LSSmOrange fusions with α-tubulin, vimentin, keratin, β-actin, α-actinin, and histone H2B localized properly in live cells and did not affect cell division (Figure S4, Supporting Information), suggesting its monomeric behavior in vivo.

To test applicability of LSSmOrange as an additional orange color for imaging with common orange and red FPs, we co-expressed its fusion constructs with those of mOrange. LSSmOrange lacks absorbance in green region and could be excited separately of mOrange. Indeed, two filter sets allowed visualization of H2B-LSSmOrange and mito-mOrange, vimentin-LSSmOrange, H2B-mOrange, mito-LSSmOrange, and cytoplasmic mOrange without cross-talk between the channels (Figure 1C).

To demonstrate suitability of LSSmOrange for multicolor applications with single-wavelength excitation, we used LSSmOrange in flow cytometry. To spectrally resolve from LSSmOrange, we have chosen three FPs: mTagBFP,[27] T-Sapphire, and LSSmKate1. All four FPs can be excited with standard violet lasers (Figure 1D). Ratios of fluorescence signals in green 546/10 nm and red 610/20 nm channels differ for each of these FPs, thus allowing their separation. Bacterial cells transformed with LSSmOrange, LSSmKate1, T-Sapphire, or mTagBFP were detected as the separate populations using 407 nm laser (Figure 1E).

3.4. Four-Color Single-Laser FCCS. To establish four-color SL-FCCS we have chosen a set of four FPs similar to that used in flow cytometry: mTagBFP2,[38] which is enhanced mTagBFP, T-Sapphire, LSSmOrange, and LSSmKate1. Figure 2A outlines the microscope setup designed for the SL-FCCS experiments. Single-laser excitation system is more suitable for multicolor FCCS analysis. Indeed, measurements with calibration dyes exhibiting cross-talk indicate that an overlap of the four detection volumes in this SL excitation system is 95−99%; that is substantially higher than for typical FCCS equipped with four different excitation lasers.

Brightness is a crucial parameter to obtain FCCS curves with high signal-to-noise ratios.[39] For the four-color SL-FCCS experiments, we selected an excitation wavelength of 440 nm, close to the absorbance maxima of the LSSmOrange and LSSmKate1. Thirty μW of 440 nm excitation provided comparable brightness of four FPs and yet minimized cross-talk and prevented photobleaching.

Because of broad emission spectra of FPs, their photons are detected in multiple channels that can result in false-positive cross-correlation. Therefore the correlation curves were corrected as outlined in the Experimental Procedures Section. In order to estimate the cross-talk intensity factors and relative molecular brightness values, the fluorescence intensities and autocorrelation curves were determined in solutions of single purified FPs or single-FP labeled beads. The measured correction values are presented in Table S1, Supporting Information. Whereas green and orange channels were dominated by T-Sapphire and LSSmOrange, respectively, blue and red channels needed to be corrected for cross-talk.

To quantify four distinct FPs in the SL-FCCS experiment, multicolored particles with the defined FP composition were prepared (Figure 2B). The control single-FP beads had in average one FP molecule per a bead. As four FPs used in the analysis exhibit different emission colors and were detected in four specific channels, below we refer to different FPs on beads as "colors". The same data traces were analyzed by photon counting histogram (PCH), single channel fluorescence correlation spectroscopy (FCS), and dual- and quadruple-FCCS.

dx.doi.org/10.1021/ja3018972 | J. Am. Chem. Soc. 2012, 134, 7913−7923

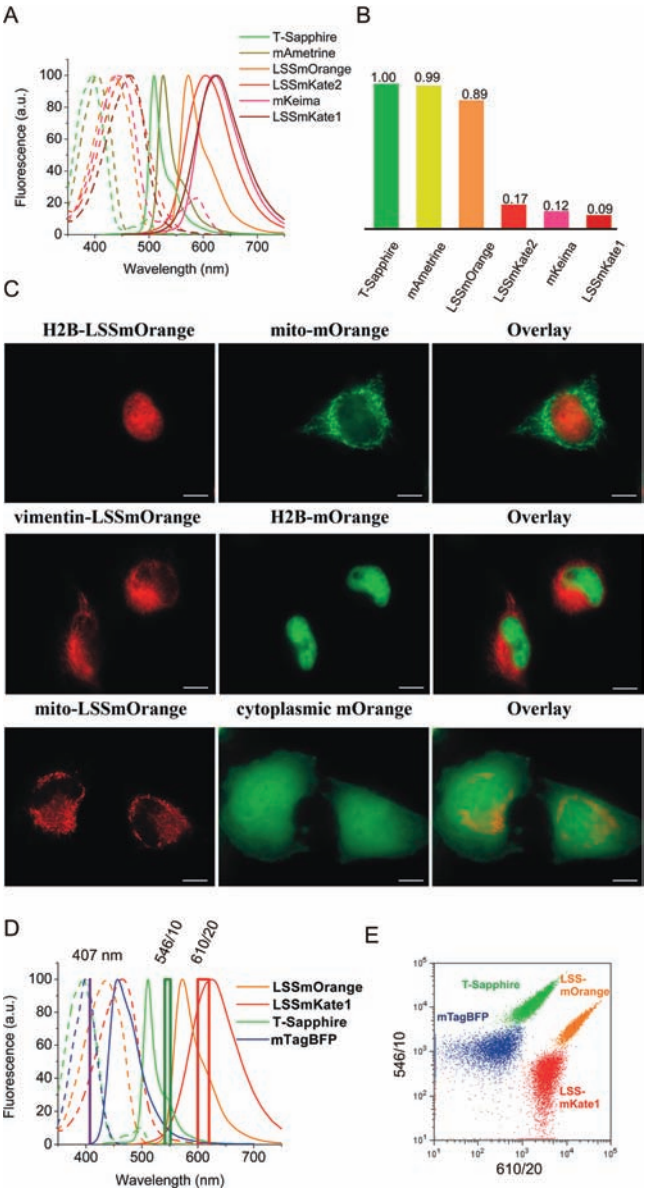

Figure 1. LSSmOrange in multicolor applications. (A) Normalized excitation (dashed lines) and emission (solid lines) spectra of all known LSS FPs: T-Sapphire (green), mAmetrine (dark yellow), LSSmOrange (orange), LSSmKate2 (red), mKeima (pink), and LSSmKate1 (brown). (B) Brightness of various LSSFPs is presented as columns of different colors. Brightness of T-Sapphire is normalized to 100%. (C) Images of coexpressed LSSmOrange and mOrange fusions in live HeLa cells. LSSmOrange fluorescence images (red, left column) were acquired using 390/40 excitation and 605/40 emission filters. mOrange fluorescence images (green, middle column) were acquired using custom orange cube with 540/20 excitation and 575/30 emission filters. The right column is an overlay of the left and middle columns. The size bars are 10 μm. Colors used are pseudocolors. (D) Normalized excitation and emission spectra of LSSmOrange, LSSmKate1, T-Sapphire, and mTagBFP and the position of the 407 nm wavelength laser line used for excitation in flow cytometry. (E) Flow cytometry analysis of bacterial cells expressing four FPs using a 407 nm laser line. Bacteria transformed with LSSmOrange, LSSmKate1, T-Sapphire, or mTagBFP were analyzed by flow cytometry for a total of 15 000 events for each type of bacterial cells.

To determine the FP stoichiometry (Figure 2C; Table S2, Supporting Information), the total brightness of beads is normalized to the brightness of control single-FP labeled beads and multiplied by the total fraction of beads with corresponding FP. The total number of particles labeled with a particular FP can be found since all the beads labeled with this FP appear the same in autocorrelation analysis. The numbers of double- and quadruple-labeled beads can be found in cross-correlation analysis. Thus, the percentage of double- and quadruple-labeled beads can be deduced for each particular FP (Figure 2C, third column).

First, two-color beads with variable FP stoichiometry and mixtures of one-color beads were analyzed. The retrieved FP stoichiometry and fractions of two-color particles were in good agreement with the compositions of FPs in the labeling protein solutions and of the beads in samples (Table S2, Supporting Information, samples 1−34). As expected for two-color beads, hardly any four-channel cross-correlating particles were detected (Figure 2C, samples 9 and 33). For double-labeled beads with equimolar ratios of FPs (positive controls) (Table S2, Supporting Information, samples 2, 12, 15, 18, 22, and 26), the expected two-channel cross-correlating particles were observed (Table S2, Supporting Information, columns F−K). For mixtures of two types of single-color beads (negative controls) cross-correlation fractions were close to zero, as expected (Table S2, Supporting Information, samples 4, 14, 16, 20, 24, and 28). Thus, cross-talk correction worked effectively. The analysis was challenging for blue-green and orange-red two-color mixtures. However, even in the cases of excess of blue and red colors, the corrected data corresponded well with the expected values (Figure 2C, samples 9 and 33).

Since FCCS experiments produced expected results for two-color beads, the quadruple-color beads were examined next. As a negative control we analyzed equimolar mixtures of single-color beads (Figure 2C, sample 44). A typical raw intensity profiles are shown as an insert in Figure 2D. Applying the cross-talk correction to the raw data, hardly any cross-correlation was observed for the negative control (Figure 2D). As the positive control we analyzed four-color beads labeled with an equimolar mixture of FPs (Figure 2C, sample 35). One can see from an insert in Figure 2E that the intensity peaks in the four individual detection traces coincided. A nonzero corrected quadruple correlation curve was obtained (Figure 2E). A cross-correlation fraction close to the expected value of 100% was observed in this case. Four-color beads with five-fold excess of one FP were also tested. Even in the cases of the excess of blue and red FPs, the analysis produced the expected results (Figure 2C, sample 36; Table S2, Supporting Information, samples 36−39).

In a four-component complex, one component may be in excess and present at the same location as the four-component complex. To model this situation, we analyzed mixtures of four-color beads with one-color beads. These mixtures demonstrated the expected decrease of the double and quadruple cross-correlation fractions (Figure 2C, samples 40−43).

3.5. Dual FRET with Single-Wavelength Excitation. LSSmOrange with its large Stokes shift emission is a putative donor for conventional red FPs. We selected mKate2[40] (ex/em 588/633 nm) as the FRET acceptor for LSSmOrange. This FRET pair is characterized by (i) substantial gap between excitation spectra of the donor and the acceptor; (ii) good separation between donor and acceptor emission; and (iii) large overlap between donor emission and acceptor absorbance (Figure 3A). A fusion protein with a caspase-3 substrate sequence (DEVD) between LSSmOrange and mKate2 was constructed. To test the LSSmOrange-mKate2 caspase-3

dx.doi.org/10.1021/ja3018972 | J. Am. Chem. Soc. 2012, 134, 7913−7923

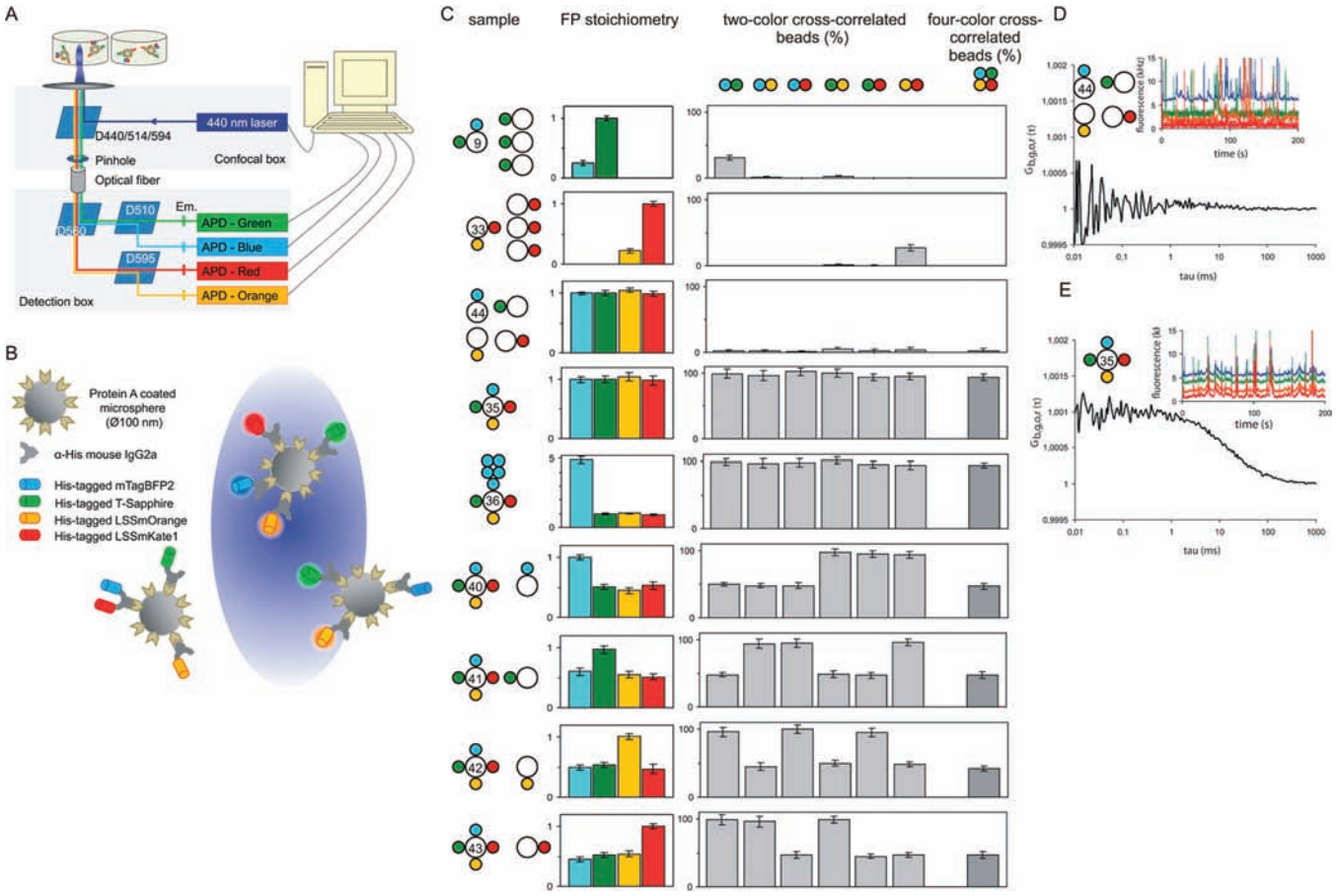

Figure 2. Four-color FCCS analysis with single-laser excitation. (A) Experimental setup. Laser light of a 440 nm diode was focused via a 60× water immersion Apochromat objective lens into the sample. Fluorescence was guided into the detection box, filtered by dichroic mirrors and emission filters (Em) and detected by four avalanche photodiode detectors. (B) FP-labeled beads used in analysis. 0.1 μm diameter protein A coated beads were labeled with anti-His mouse IgG2a antibodies. His-tagged FPs were bound to the antibody-labeled beads. Diffusion of the labeled beads through the detection volume (blue) resulted in fluorescence fluctuations, analyzed by SL-FCCS. (C) Multicolor FCCS and PCH analysis of different combinations of labeled beads. Different colors correspond to different FPs: mTagBFP2 (blue), T-Sapphire (green), LSSmOrange (orange), or LSSmKate1 (red). The first column (sample) displays the mixture composition and includes the sample number, which corresponds to the number in Table S2, Supporting Information. Samples 9 and 33 are examples of two-color beads analysis. Sample 44 (negative control) is an equimolar mixture of single-FP labeled beads. Sample 35 (positive control) consists of four-color beads labeled with equimolar mixture of four FPs. Sample 36 is an example of four-color beads with variable stoichiometry. Samples 40−43 are mixtures of single- and four-color labeled beads. The second column (FP stoichiometry) shows histograms of FP ratios in the bead mixtures. The histograms in the third column display the fractions of two- and four-color cross-correlating beads relative to the total number of detected beads in the cross-correlated channels represented by colored circles on top. The error bars in all histograms indicate the standard deviation over several independent measurements. The experimental values corresponding to the histograms and standard deviations are summarized in Table S2, Supporting Information. (D, E) The corrected four-channel cross-correlation curves for negative control (sample 44) (D) and positive control (sample 35) (E) are shown. The amplitudes are rescaled according to the cross-talk corrections. The inserts show the raw intensity profiles for the four detection channels.

biosensor, emission spectra of purified protein fusions before and after proteolysis were measured (Figure 3B). A FRET efficiency of 29% was detected.

Emission of the LSSmOrange-mKate2 FRET pair is spectrally resolvable from emission of common cyan FP-yellow FP pair (e.g., consisting of ECFP (ex/em 439/476 nm)[41] and mVenus (ex/em 515/528 nm).[42] Both FRET donors can be efficiently excited with a single wavelength of 440 nm (Figure 3C). The possibility to simultaneously image two FRET biosensors was examined in HeLa cells coexpressing a yellow cameleon 3.6 (YC3.6) calcium sensor[28] and the LSSmOrange-mKate2 caspase-3 sensor. Spectral confocal microscopy was used to acquire multichannel spectral images in real time. Obtained spectral stacks were unmixed using four reference spectra (the intact and fully cleaved caspase-3 biosensor and the Ca^{2+}-free and Ca^{2+}-bound YC3.6 sensor) (Figure 3D). Fractions of the cleaved over total caspase-3 biosensor and the calcium-bound YC3.6 over total YC3.6 sensor were calculated from the unmixed channels as outlined in the Experimental Procedures Section. Changes in Ca^{2+} concentration were induced by treatment with histamine causing repetitive and reversible release of calcium from the endoplasmic reticulum, and apoptosis was induced by treatment with TNF-α.

First, we imaged YC3.6 sensor with a control noncleavable caspase-3 biosensor (containing SASG instead of DEVD in the linker). Cells coproducing the YC3.6 and noncleavable caspase-3 biosensor showed distinct YC3.6 peaks after the addition of histamine (Figure S5, Supporting Information). Calcium spikes observed later in the experiment could result from fluctuations of calcium during apoptosis. No cleavage of control caspase-3 biosensor was detected.

dx.doi.org/10.1021/ja3018972 | J. Am. Chem. Soc. 2012, 134, 7913−7923

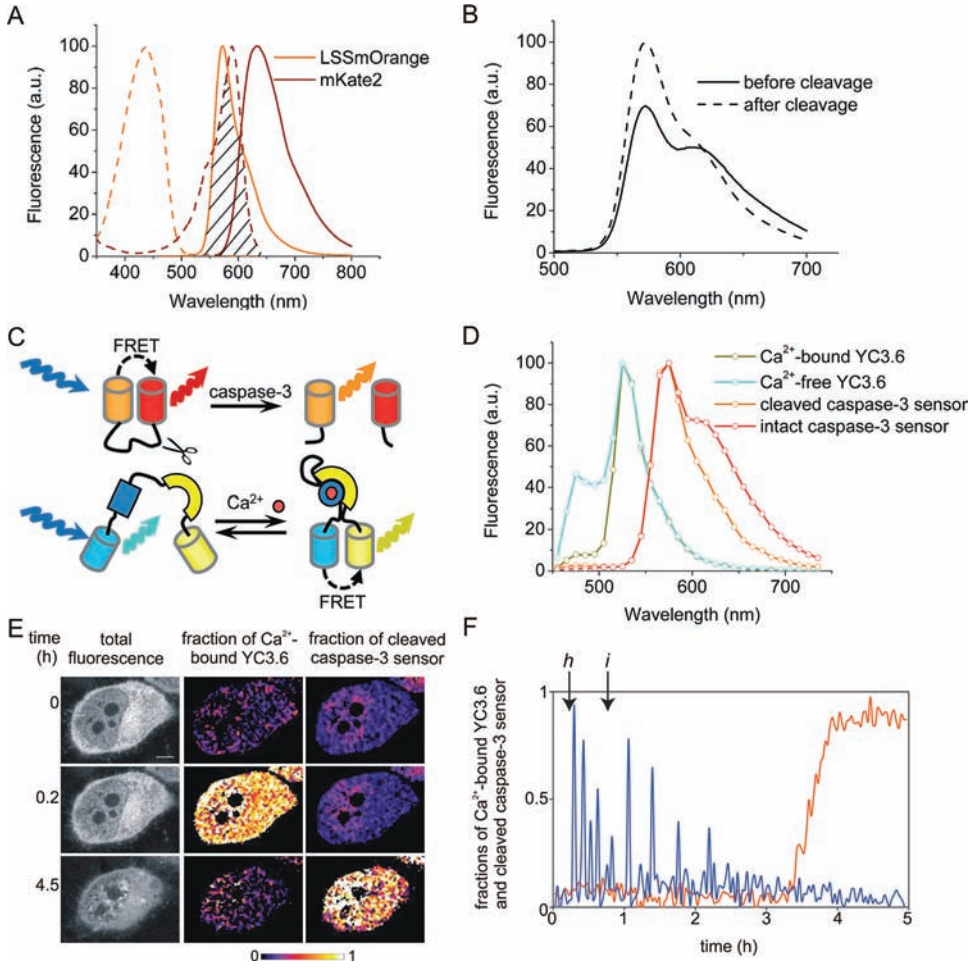

Figure 3. Dual FRET imaging using single-wavelength excitation. (A) Normalized excitation and emission spectra overlay of donor LSSmOrange and acceptor mKate2 in LSSmOrange-mKate2 FRET pair. Excitation spectra are in dashed line, and emission spectra are in solid line. (B) Emission spectra of purified LSSmOrange-DEVD-mKate2 protein fusion before and after proteolysis normalized to maximum fluorescence at 572 nm. Excitation at 440 nm was applied. (C) Schematic representation of single excitation wavelength dual FRET with two biosensors: LSSmOrange-mKate2 caspase-3 sensor (top) and CFP-YFP YC3.6 calcium sensor (bottom). (D) Reference spectra of YC3.6 in Ca^{2+}-free (cyan) and Ca^{2+}-bound (dark yellow) forms, caspase-3 sensor in intact (red), and cleaved (orange) states measured by spectral confocal imaging in HeLa cells using 29 detectors ranging from 450 to 740 nm. (E) Images of a representative HeLa cell detected at different time points in the dual-FRET imaging experiment. HeLa cells coexpressing YC3.6 sensor and LSSmOrange-mKate2 caspase-3 sensor were treated with histamine (denoted as "h") 5 min and apoptosis inducer TNF-α (denoted as "i") 30 min after starting imaging. The images of the cell show the total fluorescence intensity, the fraction of Ca^{2+}-bound over the total amount of YC3.6 sensor, and the fraction of cleaved over the total amount of caspase-3 sensor in pseudocolors. The size bar is 5 μm. (F) The relative fractions of Ca^{2+}-bound over the total amount of the YC3.6 sensor (blue) and cleaved over the total amount of the caspase-3 sensor (orange) plotted versus time.

Next, we tested performance of the functional caspase-3 LSSmOrange-mKate2 biosensor together with YC3.6 sensor. The HeLa cells co-expressing both sensors (Figure 3E) showed calcium spikes upon treatment with histamine and apoptosis induction (Figure 3F). The fraction of cleaved caspase-3 sensor was low at the start of the experiment, but after ~3.5 h, a gradual increase was observed. The fraction reached a plateau value close to 1 after 4 h indicating an almost complete cleavage of the biosensor and thus the high caspase-3 activity (Figure 3F).

3.6. Mechanism of Large Stokes Shift. The alignment of red-shifted LSSFPs (Figure S6, Supporting Information) indicated that the residues 148S and 165D found in LSSmOrange were also observed in mKeima and therefore might be critical for the LSS phenotype. To determine whether similarly to mKeima excited-state proton transfer (ESPT) occurs in LSSmOrange, we first made the S148A and D165A mutants and measured their spectral properties. In both mutants the LSS phenotype was disturbed (Figure 4A,B; Table S3, Supporting Information). Moreover, LSSmOrange/D165A displayed a regular Stokes shift (ex/em 550/565 nm) similar to mOrange. Although the mutants had very low quantum yields, their emission could be detected when excited at 440 nm. A blue-shifted peak at ~519 nm with a shoulder at ~488 nm appeared on their emission spectra (Figure 4C). Normalized excitation spectra of LSSmOrange/S148A with emission detected at 530 and 600 nm coincided with each other and excitation spectrum of LSSmOrange (Figure 4D). That suggested 440 nm light excited the same chromophore species, possibly, the protonated form of the chromophore. However, because ESPT was disrupted only residual fluorescence was observed in LSSmOrange/S148A.

We next studied isotope and temperature dependencies of LSSmOrange fluorescence. The emission spectra were measured at room (298 K) and liquid nitrogen (77 K)

dx.doi.org/10.1021/ja3018972 | J. Am. Chem. Soc. 2012, 134, 7913−7923

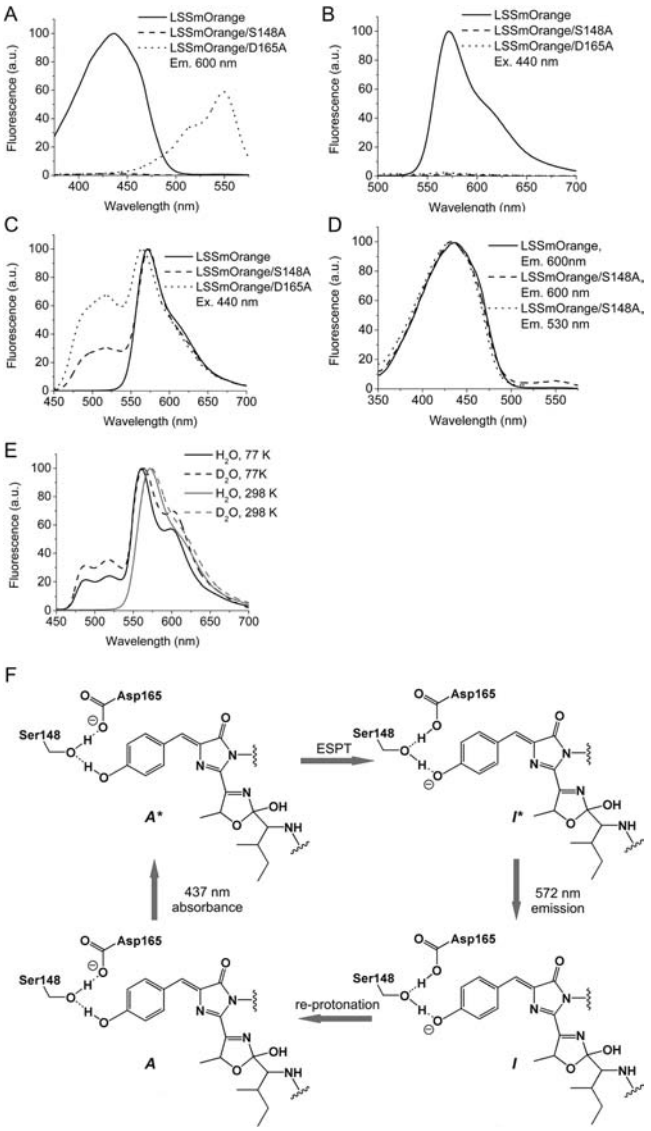

Figure 4. The large Stokes shift phenotype of LSSmOrange. (A,B) Overlay of excitation (A) and emission (B) spectra of LSSmOrange (solid line), LSSmOrange/S148A (dashed line), and LSSmOrange/D165A (dotted line). Equal concentrations of purified proteins (0.15 mg/mL) were analyzed. Excitation spectra were recorded using emission at 600 nm. Emission spectra were detected at 440 nm excitation. (C) Overlay of normalized emission spectra of LSSmOrange (solid line), LSSmOrange/S148A (dashed line), and LSSmOrange/D165A (dotted line). Excitation at 440 nm was applied. (D) Overlay of normalized excitation spectra detected at 600 nm for LSSmOrange (solid line), detected at 600 nm for LSSmOrange/S148A (dashed line), and detected at 530 nm for LSSmOrange/S148A (dotted line). (E) Normalized emission spectra of LSSmOrange in two different solvents (H_2O and D_2O) at 77 and 298 K. The samples were excited at 440 nm. (F) Proposed photocycle for LSSmOrange at room temperature. Excitation light (maximum at 437 nm) transfers the ground state of the neutral chromophore (compound A) into excited state (compound A*). Then A* is transformed by ESPT into the intermediate excited state denoted as the compound I*. I* emits photon (anionic form of the chromophore, emission maximum at 572 nm). After that a proton transfer from Asp165 via Ser148 to the chromophore regenerates the ground state (compound A) of the neutral chromophore.

temperatures (Figure 4E). At 77 K, the LSSmOrange emission spectra had blue-shifted peaks at ~519 and ~488 nm. Both peaks were equally enhanced by deuterium substitution. Since ESPT efficiency is reduced at low temperatures, the blue-shifted emission can be assigned to the protonated form of the chromophore. Similar effect has been observed for red LSSFPs.[36,43] Overall this suggested that in LSSmOrange, a proton relay involves residues 148S and 165D and is responsible for the ESPT process resulting in the LSS phenotype. The proposed LSSmOrange photocycle is shown in Figure 4E.

4. DISCUSSION

LSSmOrange differs from parental mOrange by six amino acid substitutions. During random mutagenesis, the mutations I165D and M167L were persistent in the best mutants selected for the next mutagenesis rounds. We demonstrated that one of these residues, 165D, together with residue 148S, which was present in mOrange, is implicated in ESPT. The ESPT process has been shown to be crucial for the LSS phenotypes in other LSSFPs including mKeima,[43] LSSmKates,[36] and wild-type GFP.[44] The common mechanism implies that the chromophore is initially protonated. Upon excitation, proton transfer from the hydroxyl group of the chromophore takes place, and the anionic chromophore intermediate emits a photon.[44,45] Our data indicate that LSSmOrange has a proton relay pathway similar to that of mKeima.

Multicolor FCCS analysis of higher order molecular conglomerates at a single-molecule level has been a desirable technique. Its combination with genetically encoded probes should enable to study large intracellular protein complexes. We expanded previously available two-color FP-based SL-FCCS approach[6,11] to four-color SL-FCCS combined with PCH technique. The four-color analysis was possible because LSSmOrange emission is resolvable with emission of red LSSmKate1 as well as with emission of blue TagBFP2 and green T-Sapphire. Because the excitation confocal volume of all four FPs is identical, the four-color SL-FCCS provides straightforward, robust calibration and highly quantitative data on comigration of single particles composed of up to four species with variable stoichiometry. Although FCCS in vivo applications are beyond the scope of this paper, the establishment of this technique opens the way to spatiotemporal studies of protein complexes in live cells.

The simultaneous real-time imaging of two FRET biosensors is a useful approach for studying relative kinetics of two biological processes.[4,5] Comparing to the reported strategies for dual biosensor imaging,[18−20] the approach presented here has several advantages. In contrast to the technique[18] where two donors should have been excited separately, the combination of the LSSmOrange-mKate2 and CFP-YFP FRET pairs has enabled to use a single-laser that efficiently excites both FRET donors at their excitation maxima. Comparing to the Sirius-mseCFP and Sapphire-DsRed FRET pairs that also enable single-wavelength excitation,[19] both FRET pairs in this paper are characterized by red-shifted excitation and emission that result in reduced autofluorescence, smaller light-scattering, and lower phototoxicity at longer wavelengths. Moreover, the emission spectra of the LSSmOrange-mKate2 and cyan FP-yellow FP pairs are well separated, thus allowing their use without precise adjustment of a stoichiometry of the biosensors or intracellular separation of their localization. Lastly, the large Stokes shift of LSSmOrange is advantageous to make it a donor in a FRET pair because it provides much less acceptor cross-excitation, which is a problem in other orange-red FRET pairs.

dx.doi.org/10.1021/ja3018972 | J. Am. Chem. Soc. 2012, 134, 7913−7923

5. CONCLUSIONS

In summary, LSSmOrange fills up the spectral gap between yellow and red LSSFPs and allows for numerous multicolor applications using the single-wavelength excitation. These applications, among others, include four-color cell and protein labeling in flow cytometry and microscopy, four-color FCCS using solely genetically encoded FPs, and intracellular imaging of two FRET pairs including the common CFP-YFP pair. Use of a single excitation wavelength also provides the possibility to study several fast processes in real time. The advantages of LSSmOrange broaden possibilities of fast multicolor imaging and make it a probe of choice to truly simultaneously track and quantify multiple populations of intracellular objects, to detect brief protein colocalization and interaction events, and to study relationship between several biochemical activities in a live cell.

■ ASSOCIATED CONTENT

Supporting Information

Six supporting figures and three supporting tables are available. Alignment of the amino acid sequences of LSSmOrange, mOrange, and EGFP. Biochemical and photobleaching properties of LSSmOrange and other available LSSFPs. Polyacrylamide gel with purified LSSmOrange, mOrange, and LSSmKate2. Fluorescence images of the LSSmOrange fusion constructs in live mammalian cells. Single-wavelength excitation dual FRET with the YC3.6 sensor and control noncleavable caspase-3 biosensor. Alignment of the amino acid sequences of red-shifted LSSFPs. Molecular brightness and cross-talk factors of FPs used in four-color FCCS analysis. Multicolor FCCS analysis of 100 nm beads labeled with four FPs in different ratios. Spectral properties of the LSSmOrange/S148A and LSSmOrange/D165A mutants. This material is available free of charge via Internet at http://pubs.acs.org.

■ AUTHOR INFORMATION

Corresponding Author

vladislav.verkhusha@einstein.yu.edu

Author Contributions

[§]These authors contributed equally.

Notes

The authors declare no competing financial interest.

■ ACKNOWLEDGMENTS

We thank J. Zhang for the assistance with flow cytometry, M.W. Davidson (Florida State University, FL) for the mammalian plasmids with protein fusions, and R.E. Campbell (University of Alberta, Canada) for the genes of fluorescent proteins. This work was supported by Middelgroot investment grants 834.09.003 and 834.07.003 of The Netherlands Organization for Scientific Research (NWO) (to T.W.J.G.) and by grants GM073913 and CA164468 from the US National Institutes of Health (to V.V.V.).

■ REFERENCES

(1) Chudakov, D. M.; Matz, M. V.; Lukyanov, S.; Lukyanov, K. A. *Physiol. Rev.* **2010**, *90*, 1103.

(2) Wu, B.; Piatkevich, K. D.; Lionnet, T.; Singer, R. H.; Verkhusha, V. V. *Curr. Opin. Cell. Biol.* **2011**, *23*, 310.

(3) Haustein, E.; Schwille, P. *Annu. Rev. Biophys. Biomol. Struct.* **2007**, *36*, 151.

(4) Schultz, C.; Schleifenbaum, A.; Goedhart, J.; Gadella, T. W. J., Jr. *ChemBioChem* **2005**, *6*, 1323.

(5) Carlson, H. J.; Campbell, R. E. *Curr. Opin. Biotechnol.* **2009**, *20*, 19.

(6) Bacia, K.; Kim, S. A.; Schwille, P. *Nat. Methods* **2006**, *3*, 83.

(7) Slaughter, B. D.; Li, R. *Mol. Biol. Cell* **2010**, *21*, 4306.

(8) Galperin, E.; Verkhusha, V. V.; Sorkin, A. *Nat. Methods* **2004**, *1*, 209.

(9) Sun, Y.; Wallrabe, H.; Booker, C. F.; Day, R. N.; Periasamy, A. *Biophys. J.* **2010**, *99*, 1274.

(10) Heinze, K. G.; Koltermann, A.; Schwille, P. *Proc. Natl. Acad. Sci. U.S.A.* **2000**, *97*, 10377.

(11) Kogure, T.; Karasawa, S.; Araki, T.; Saito, K.; Kinjo, M.; Miyawaki, A. *Nat. Biotechnol.* **2006**, *24*, 577.

(12) Stasevich, T. J.; Mueller, F.; Michelman-Ribeiro, A.; Rosales, T.; Knutson, J. R.; McNally, J. G. *Biophys. J.* **2010**, *99*, 3093.

(13) Heinze, K. G.; Jahnz, M.; Schwille, P. *Biophys. J.* **2004**, *86*, 506.

(14) Hwang, L. C.; Gosch, M.; Lasser, T.; Wohland, T. *Biophys. J.* **2006**, *91*, 715.

(15) Burkhardt, M.; Heinze, K. G.; Schwille, P. *Opt. Lett.* **2005**, *30*, 2266.

(16) VanEngelenburg, S. B.; Palmer, A. E. *Curr. Opin. Chem. Biol.* **2008**, *12*, 60.

(17) Ibraheem, A.; Campbell, R. E. *Curr. Opin. Chem. Biol.* **2010**, *14*, 30.

(18) Ai, H. W.; Hazelwood, K. L.; Davidson, M. W.; Campbell, R. E. *Nat. Methods* **2008**, *5*, 401.

(19) Tomosugi, W.; Matsuda, T.; Tani, T.; Nemoto, T.; Kotera, I.; Saito, K.; Horikawa, K.; Nagai, T. *Nat. Methods* **2009**, *6*, 351.

(20) Niino, Y.; Hotta, K.; Oka, K. *PLoS One* **2009**, *4*, e6036.

(21) Zapata-Hommer, O.; Griesbeck, O. *BMC Biotechnol.* **2003**, *3*, 5.

(22) Piatkevich, K. D.; Hulit, J.; Subach, O. M.; Wu, B.; Abdulla, A.; Segall, J. E.; Verkhusha, V. V. *Proc. Natl. Acad. Sci. U S A* **2010**, *107*, 5369.

(23) Shaner, N. C.; Campbell, R. E.; Steinbach, P. A.; Giepmans, B. N.; Palmer, A. E.; Tsien, R. Y. *Nat. Biotechnol.* **2004**, *22*, 1567.

(24) Ho, S. N.; Hunt, H. D.; Horton, R. M.; Pullen, J. K.; Pease, L. R. *Gene* **1989**, *77*, 51.

(25) Verkhusha, V. V.; Lukyanov, K. A. *Nat. Biotechnol.* **2004**, *22*, 289.

(26) Gross, L. A.; Baird, G. S.; Hoffman, R. C.; Baldridge, K. K.; Tsien, R. Y. *Proc. Natl. Acad. Sci. U.S.A.* **2000**, *97*, 11990.

(27) Subach, O. M.; Gundorov, I. S.; Yoshimura, M.; Subach, F. V.; Zhang, J.; Gruenwald, D.; Souslova, E. A.; Chudakov, D. M.; Verkhusha, V. V. *Chem. Biol.* **2008**, *15*, 1116.

(28) Nagai, T.; Yamada, S.; Tominaga, T.; Ichikawa, M.; Miyawaki, A. *Proc. Natl. Acad. Sci. U.S.A.* **2004**, *101*, 10554.

(29) Chen, Y.; Muller, J. D.; So, P. T.; Gratton, E. *Biophys. J.* **1999**, *77*, 553.

(30) Haupts, U.; Maiti, S.; Schwille, P.; Webb, W. W. *Proc. Natl. Acad. Sci. U.S.A.* **1998**, *95*, 13573.

(31) Maeder, C. I.; Hink, M. A.; Kinkhabwala, A.; Mayr, R.; Bastiaens, P. I.; Knop, M. *Nat. Cell Biol.* **2007**, *9*, 1319.

(32) Haustein, E.; Schwille, P. *Curr. Opin. Struct. Biol.* **2004**, *14*, 531.

(33) Palo, K.; Mets, U.; Jager, S.; Kask, P.; Gall, K. *Biophys. J.* **2000**, *79*, 2858.

(34) Huang, B.; Perroud, T. D.; Zare, R. N. *ChemPhysChem* **2004**, *5*, 1523.

(35) Perroud, T. D.; Huang, B.; Zare, R. N. *ChemPhysChem* **2005**, *6*, 905.

(36) Piatkevich, K. D.; Malashkevich, V. N.; Almo, S. C.; Verkhusha, V. V. *J. Am. Chem. Soc.* **2010**, *132*, 10762.

(37) Shaner, N. C.; Lin, M. Z.; McKeown, M. R.; Steinbach, P. A.; Hazelwood, K. L.; Davidson, M. W.; Tsien, R. Y. *Nat. Methods* **2008**, *5*, 545.

(38) Subach, O. M.; Cranfill, P. J.; Davidson, M. W.; Verkhusha, V. V. *PLoS One* **2011**, *6*, e28674.

(39) Koppel, D. E. *Phys. Rev. A* **1974**, *10*, 1938.

(40) Shcherbo, D.; Murphy, C. S.; Ermakova, G. V.; Solovieva, E. A.; Chepurnykh, T. V.; Shcheglov, A. S.; Verkhusha, V. V.; Pletnev, V. Z.;

Hazelwood, K. L.; Roche, P. M.; Lukyanov, S.; Zaraisky, A. G.; Davidson, M. W.; Chudakov, D. M. *Biochem. J.* **2009**, *418*, 567.
(41) Llopis, J.; McCaffery, J. M.; Miyawaki, A.; Farquhar, M. G.; Tsien, R. Y. *Proc. Natl. Acad. Sci. U.S.A.* **1998**, *95*, 6803.
(42) Nagai, T.; Ibata, K.; Park, E. S.; Kubota, M.; Mikoshiba, K.; Miyawaki, A. *Nat. Biotechnol.* **2002**, *20*, 87.
(43) Henderson, J. N.; Osborn, M. F.; Koon, N.; Gepshtein, R.; Huppert, D.; Remington, S. J. *J. Am. Chem. Soc.* **2009**, *131*, 13212.
(44) Chattoraj, M.; King, B. A.; Bublitz, G. U.; Boxer, S. G. *Proc. Natl. Acad. Sci. U.S.A.* **1996**, *93*, 8362.
(45) van Thor, J. J. *Chem. Soc. Rev.* **2009**, *38*, 2935.